magnetization process can be considered as being reversible in temperature. From the magnetization curve at 5 K, the saturation magnetization was determined as 3.9 μ_B per formula unit. This high magnetization originates from the parallel alignment of the Mn and Fe moments, though the moments of Mn are much larger than those of Fe (ref. 12). Variation of the Mn/Fe ratio may also be used to further improve the MCE.

The magnetic entropy changes, ΔS_m, are calculated from magnetization data by means of the equation

$$\Delta S_m(T,B) = S_m(T,B) - S_m(T,0) = \int_0^B \left(\frac{\partial M}{\partial T}\right)_{B'} \mathrm{d}B'$$

which is based on a Maxwell relation. The results are shown in Fig. 3. The calculated maximum values of the magnetic entropy changes are 14.5 J kg^{-1} K^{-1} and 18 J kg^{-1} K^{-1} for field changes from 0 to 2 T and 0 to 5 T, respectively. The maximum magnetic entropy in 3*d* materials depends on the spin moment *S*. Because there are two magnetic ions per formula unit, we have $S_m = 2R\ln(2S + 1)$, where *R* is the universal gas constant. From the saturation magnetic moment, we estimate the average *S* value of the magnetic ions to be 1, thus $S_m = 18.3$ J mol^{-1} K^{-1} = 117 J kg^{-1} K^{-1}, which is about 6 times larger than the value obtained from the magnetization measurements. For comparison, the magnetic entropy change of the compound $Gd_5Ge_2Si_2$ and Gd is also shown in Fig. 3. It is evident that the MCE in $MnFeP_{1-x}As_x$ compounds is comparable with that of $Gd_5Ge_2Si_2$, though the Gd compound has a larger magnetic moment at 5 K. The origin of the large magnetic entropy change is in the comparatively high 3*d* moments and in the rapid change of magnetization in the field-induced magnetic phase transition. In rare-earth materials, the magnetic moment fully develops only at low temperatures, and therefore the entropy change near room temperature is only a fraction of the potential value. In 3*d* compounds, the strong magneto-crystalline coupling results in competing intra- and inter-atomic interactions, and leads to a modification of metal–metal distances which may change the iron and manganese magnetic moments and favour spin ordering.

The excellent magnetocaloric features of the compound $MnFeP_{0.45}As_{0.55}$, in addition to the very low material costs, make it an attractive candidate material for a commercial magnetic refrigerator. □

Received 30 July; accepted 6 November 2001.

1. Glanz, J. Making a bigger chill with magnets. *Science* **279,** 2045 (1998).
2. Pecharsky, V. K. & Gschneidner, K. A. Jr Giant magnetocaloric effect in $Gd_5(Si_2Ge_2)$. *Phys. Rev. Lett.* **78,** 4494–4497 (1997).
3. Gschneidner, K. A. Jr *et al.* Recent developments in magnetic refrigeration. *Mater. Sci. Forum* **315–317,** 69–76 (1999).
4. Zimm, C. *et al.* Description and performance of a near-room temperature magnetic refrigerator. *Adv. Cryogen. Eng.* **43,** 1759–1766 (1998).
5. Tishin, A. M. in *Handbook of Magnetic Materials* Vol. 12 (ed. Buschow, K. H. J.) 395–524 (North Holland, Amsterdam, 1999).
6. Choe, W. *et al.* Making and breaking covalent bonds across the magnetic transition in the giant magnetocaloric material $Gd_5(Si_2Ge_2)$. *Phys. Rev. Lett.* **84,** 4617–4620 (2000).
7. Giguere, A. *et al.* Direct measurement of the "giant" adiabatic temperature change in $Gd_5(Si_2Ge_2)$. *Phys. Rev. Lett.* **83,** 2262–2265 (1999).
8. Morellon, L. *et al.* Nature of the first-order antiferromagnetic-ferromagnetic transition in the Ge-rich magnetocaloric compounds $Gd_5(Si_xGe_{1-x})_4$. *Phys. Rev. B* **62,** 1022–1026 (2000).
9. Pytlik, L. & Zieba, A. Magnetic phase diagram of MnAs. *J. Magn. Magn. Mater.* **51,** 199–210 (1985).
10. Zach, R., Guillot, M. & Fruchart, R. The influence of high magnetic fields on the first order magneto-elastic transition in $MnFe(P_{1-y}As_y)$ systems. *J. Magn. Magn. Mater.* **89,** 221–228 (1990).
11. Bacmann, M. *et al.* Magnetoelastic transition and antiferro-ferromagnetic ordering in the system $MnFeP_{1-y}As_y$. *J. Magn. Magn. Mater.* **134,** 59–67 (1994).
12. Beckman, O. & Lundgren, L. in *Handbook of Magnetic Materials* (ed. Buschow, K. H. J.) Vol. 6, 181–287 (North Holland, Amsterdam, 1991).

Acknowledgements

We thank A.J. Riemersma for preparation of graphs. Part of this work was performed within the scientific exchange program between the Netherlands and China. This work was financially supported by the Dutch Technology Foundation STW.

Correspondence and requests for materials should be addressed to E.B. (e-mail: bruck@wins.uva.nl).

Remote electronic control of DNA hybridization through inductive coupling to an attached metal nanocrystal antenna

Kimberly Hamad-Schifferli*, John J. Schwartz†, Aaron T. Santos*, Shuguang Zhang‡ & Joseph M. Jacobson*

** The Media Laboratory and the ‡Center for Biomedical Engineering, Massachusetts Institute of Technology, 77 Massachusetts Ave., Cambridge, Massachusetts 02139, USA*

† Engeneos, 40 Bear Hill Road, Waltham, Massachusetts 02451, USA

Increasingly detailed structural[1] and dynamic[2,3] studies are highlighting the precision with which biomolecules execute often complex tasks at the molecular scale. The efficiency and versatility of these processes have inspired many attempts to mimic or harness them. To date, biomolecules have been used to perform computational operations[4] and actuation[5], to construct artificial transcriptional loops that behave like simple circuit elements[6,7] and to direct the assembly of nanocrystals[8]. Further development of these approaches requires new tools for the physical and chemical manipulation of biological systems. Biomolecular activity has been triggered optically through the use of chromophores[9–14], but direct electronic control over biomolecular 'machinery' in a specific and fully reversible manner has not yet been achieved. Here we demonstrate remote electronic control over the hybridization behaviour of DNA molecules, by inductive coupling of a radio-frequency magnetic field to a metal nanocrystal covalently linked to DNA[15]. Inductive coupling to the nanocrystal increases the local temperature of the bound DNA, thereby inducing denaturation while leaving surrounding molecules relatively unaffected. Moreover, because dissolved biomolecules dissipate heat in less than 50 picoseconds (ref. 16), the switching is fully reversible. Inductive heating of macroscopic samples is widely used[17–19], but the present approach should allow extension of this concept to the control of hybridization and thus of a broad range of biological functions on the molecular scale.

Inductive coupling is the transfer of energy between circuits. If the secondary circuit has finite impedance, eddy currents are produced which are converted to heat by the Joule effect[17]. Heating a conductor by placing it in an alternating magnetic field is generally used to heat macroscopic samples. Here we apply it to metallic nanocrystals (diameter 1.4 nm) in solution. Induction heating is accompanied by a skin-depth effect, resulting from partial cancellation of the magnetic fields. Consequently, most of the power absorbed by the conductor is concentrated in a depth d_0, given by:

$$d_0 = \frac{1}{2\pi}\sqrt{\frac{\rho 10^7}{\mu_r \mu_0 f}} \quad (1)$$

where μ_r is magnetic permeability, μ_0 is the permeability of free space, ρ is the material resistivity, and f is the frequency of the alternating magnetic field. The power density P is given by:

$$P = 4\pi H_c^2 \mu_0 \mu_r f F \frac{d_0}{d} \quad (2)$$

where d is the sample diameter, H_e is the magnetic field strength, and F is a transmission factor that has a sigmoidal dependence on d/d_0. Optimal power absorption and heating occur when $d/d_0 = 3.5$. To optimally heat by induction a gold nanocrystal with $d = 1.4$ nm, $f = 49$ GHz (radio frequency range) is required[17,18]. Here we use

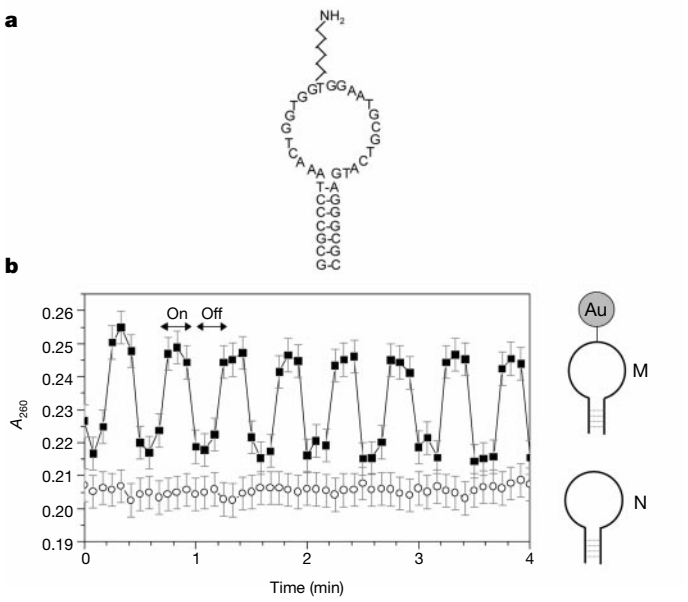

Figure 1 Inductive coupling to nanocrystals linked to DNA and evidence of dehybridization. **a**, Sequence of the hairpin molecule, M. The molecule is self-complementary at the ends for 7 bases, with a primary amine in the loop to which a 1.4-nm gold nanocrystal is covalently linked. **b**, Absorbance at 260 nm (A_{260}) of a solution of M in RFMF (squares). Arrows indicate when the RFMF is on/off. Circles, response of N (no nanocrystals) in RFMF. Gold nanocrystals also show an absorbance increase under RFMF, qualitatively attributed to the change in the optical absorption due to eddy currents. However, the absorbance increases nearly uniformly over 200–300 nm with RFMF and is small relative to the oligo change in absorbance. To obtain the data shown here, the nanocrystal contribution was subtracted (see Supplementary Information for details). M with a fluorophore/quencher pair on the ends shows fluorescence increasing reversibly with RFMF (not shown), confirming dehybridization.

f = 1 GHz, which results in a skin depth larger than the particle so that the entire particle is heated. We note that additional mechanisms, including induced dipole torque on the nanoparticle which increases the kinetic energy of the nanoparticles, may be important at these length scales. The physics of heating nanometre particles has not been explored previously, and will be the subject of future investigations. There are numerous examples of the heating of magnetic particles by a magnetic field for the treatment of tumours through macroscopic tissue heating[19]. However, we emphasize that the (magnetite) particles in such cases are several orders of magnitude larger in volume than the particles used in our investigation, and are not interfaced to individual molecules.

In order to demonstrate reversible electronic control, we have constructed a DNA hairpin-loop oligonucleotide covalently linked to a nanometre scale antenna. 38-nucleotide hairpin-loop DNA which is self-complementary at each end for 7 bases[20] (Fig. 1a) was covalently linked to a 1.4-nm gold nanocrystal by a primary amine appended to a single base[21–24]. Because of the loop constraint, the DNA rehybridizes on a timescale comparable to dehybridization[25]. The dehybridization was monitored by the hyperchromicity of DNA, measured by optical absorbance at 260 nm (A_{260})[26]. A solution of the nanocrystal-linked oligonucleotides (referred to as M) was put into a radio-frequency magnetic field (RFMF) with f = 1 GHz. A_{260} was monitored in an ultraviolet–visible spectro-

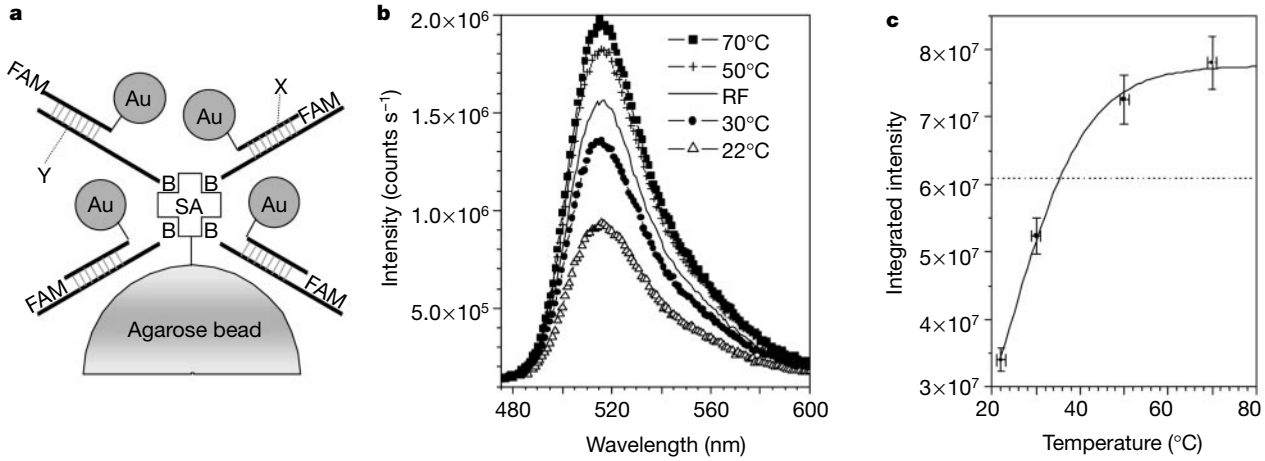

Figure 2 Determination of effective temperature from inductive coupling to a gold nanocrystal linked to DNA. **a**, The two-phase system. X is a 12-nucleotide DNA molecule covalently labelled with a gold nanocrystal on its 3′ end and the fluorophore FAM on its 5′ end. Its complementary strand Y has biotin (B) on the 5′ end, which was captured onto agarose beads with streptavidin (SA) on the surface. Once X dehybridizes from Y it can diffuse into the supernatant. **b**, Supernatant fluorescence spectra. Each sample is subject to a fixed temperature (22 °C, 30 °C, 50 °C, 70 °C) or RFMF (solid line). **c**, Integrated peak intensity of the supernatant fluorescence spectra shown in **b** (circles) and a sigmoidal fit (solid line), and the intensity of the sample exposed to RFMF (dotted line). Extrapolation of RFMF sample intensity results in an effective temperature of 35 °C for X.

photometer as the RFMF was pulsed at 15-s intervals (Fig. 1b). As the RFMF was switched on, A_{260} increased from 0.22 to 0.25, indicating that M dehybridized with the RFMF (squares in Fig. 1b). When the RFMF was switched off, A_{260} returned to its original value. Cycling through the on and off states was repeatable. The on/off ratio of A_{260} is 1.09, consistent with calculated absorption coefficients for this sequence hybridizing and dehybridizing 7 bases. Control solutions with DNA only (that is, not linked to gold nanocrystals), referred to as N, resulted in no change in the absorbance with RFMF (circles in Fig. 1b). This shows that inductive coupling to a covalently bound metal nanocrystal can reversibly dehybridize DNA on a timescale of at most several seconds.

To determine the effective temperature that inductive coupling to the nanocrystal produces locally, we designed a two-phase system in which DNA is dehybridized from a solid support into solution (Fig. 2a). X is a 12-nucleotide DNA molecule with a nanocrystal on the 3′ end and a fluorophore (FAM) on the 5′ end (see Methods). It was hybridized to its complement Y, which was immobilized onto 100-μm streptavidin-coated agarose beads comprising the solid phase. As X dehybridizes from Y, it diffuses into the supernatant. The amount of dehybridization is proportional to the amount of X in the supernatant, which was measured by fluorescence spectroscopy. One aliquot of the sample was exposed to the RFMF and its supernatant removed. Its fluorescence spectrum was compared to supernatants of aliquots thermally heated at specific temperatures. The intensity of the supernatant fluorescence spectra (Fig. 2b) increases with temperature, indicative of increased amounts of X dehybridized. The sample exposed to RFMF has intensity (solid line) in between the 30 °C and 50 °C samples. The integrated peak intensity of the spectra (Fig. 2c) as a function of temperature (squares) can be fitted to a sigmoidal (solid line), corresponding to a thermal denaturation curve. The intensity of the RFMF sample (dashed line) extrapolates to 35 °C, indicating that the effective temperature increase on X produced by the RFMF is +13 °C. This change in temperature is sufficient for control of many biological processes.

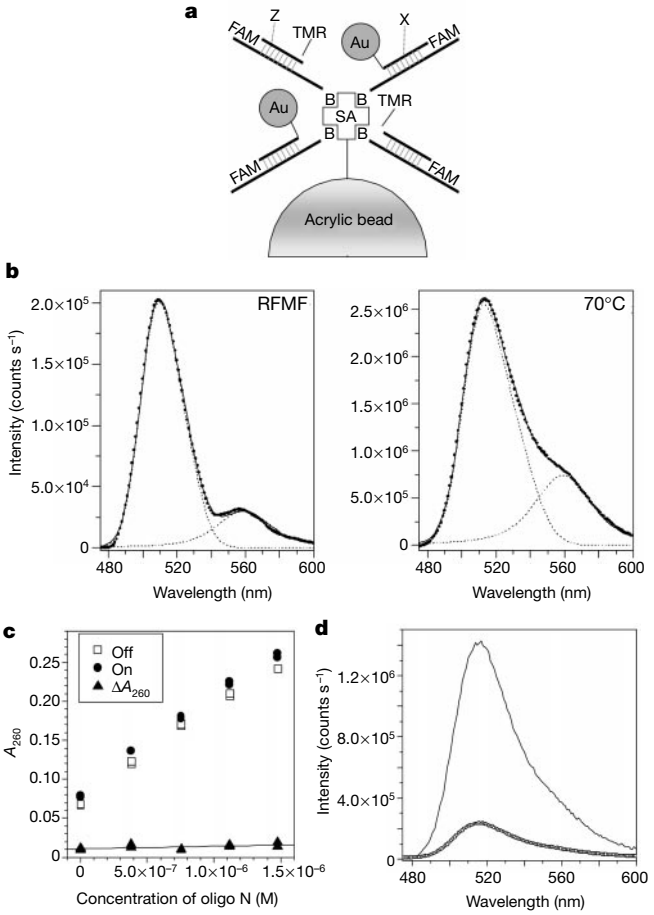

Figure 3 Testing selectivity. **a**, Two-phase system. Z is identical to X but has the fluorophore TMR on the 3′ end (λ_{max} = 563 nm). The beads have both X-Y and Z-Y hybrids. **b**, Difference fluorescence spectra (dots) (after dehybridization by heat/RFMF minus before dehybridization) scaled to same height. Shown are individual fluorescence peak fits (dashed lines) and composite fits (solid lines). When fitting the experimental data obtained upon RFMF and heat exposure, two spectral peaks centred at 516 nm and 563 nm and having full-widths at half-maximum of 31 nm and 38 nm, respectively, were used in each case. Sample exposed to RFMF (left) and to 70 °C (right). **c**, A_{260} of M and N mixture with RFMF on (circles) and off (squares), ΔA_{260} (triangles), and fit (line) as a function of N concentration. The concentration of M is 1.12×10^{-7} M while N ranges from 0 to 1.4×10^{-6} M. Based on concentrations the estimated density is ~1 molecule per 10^6 nm^3, an upper limit on intermolecular separation as it does not account for diffusion. **d**, Spectra of supernatants with one (dots) or two (line) RFMF dehybridizations normalized to the intensity of the 70 °C aliquot for each sample.

One important property is the ability to address molecules with a nanocrystal while having a lesser effect on molecules not bound to a nanocrystal. If induction heating of the nanocrystal is sufficiently spatially localized, it will afford selectivity. We used a two-phase system in which X was mixed with Z, identical in sequence to X but instead has TMR (see Methods) on the 3′ end (Fig. 3a). TMR emits at a wavelength distinct from FAM (λ_{max} = 563 nm). The two-phase system comprises tetrameric avidin acrylic beads with both X-Y and Z-Y hybrids on the surface in approximately equimolar amounts. One sample was exposed to RFMF, and the supernatant was compared to a thermally heated sample (70 °C) by fluorescence. The difference of the spectrum before and after dehybridization for the 70 °C sample (Fig. 3b, right) has peaks at 515 nm and 563 nm, indicating dehybridization of both X and Z. The RFMF sample (Fig. 3b, left) shows intensity at 515 nm due to dehybridized X but negligible intensity at 563 nm, which indicates selectivity: Z is relatively unaffected by induction heating of X in its proximity. Quantification of the spectra yields ~80% X for the RFMF sample and ~55% for the 70 °C sample. The slight amount of Z dehybridized in the RFMF sample is presumably due to the proximity of the molecules associated with tetrameric avidin (intermolecular separation is expected to be ≥ 10 nm).

RFMF experiments on solutions of mixtures of M and N also illustrate selective heating. Figure 3c shows A_{260} with RFMF on and off for a fixed concentration of M as N was added. Values of A_{260} for the on and off states increase linearly, but the difference (ΔA_{260}) remains constant. Samples of increasing concentration of M show ΔA_{260} increasing with concentration (not shown). These experiments indicate that induction heating of the nanocrystal on M is sufficiently localized that N is unaffected. Another indication of selectivity of RFMF dehybridization is evident in the purification of gold-linked X from unlabelled X, where the fraction of gold-linked oligonucleotides increases with successive RFMF dehybridizations. Figure 3d shows the fluorescence spectra of a sample before and after RFMF purification. A sample of partially labelled X is RFMF dehybridized and compared to a 70 °C aliquot, which effectively provides the total number of X in the system (dots). If the RFMF supernatant is rehybridized to Y and RFMF dehybridized a second time, its intensity is higher relative to the 70 °C aliquot (lines). The percentage of molecules dehybridized by RFMF increases after purification, suggesting the RFMF preferentially dehybridizes X linked with nanocrystals. If RFMF dehybridization were non-selective, this percentage would be the same for both samples. These experiments show that induction heating of the nanocrystal is localized such that surrounding molecules are not substantially affected.

Manipulation of DNA by itself is useful, as it has potential as an

actuator[5] and performing computations[27]. Because nanocrystals can be readily attached to proteins, switching more complex processes—such as enzymatic activity (S.Z., J. Shi, M. Jura, K.H.-S., J.J.S. and J.M.J, manuscript in preparation), biomolecular assembly, gene regulation, and protein function—might be possible. Due to the spatial localization of denaturation, it might be possible to control portions of proteins or nucleic acids while the rest of the molecule and neighbouring species would remain relatively unaffected. Control of dehybridization of antisense oligos in transcription[28] would permit reversible control of the production of specific messenger RNA. Because the addressing is not optical, this technology could be useful in highly scattering media. □

Methods

Linking gold nanocrystals to DNA hairpin-loop molecules

DNA oligonucleotides were synthesized via solid-phase synthesis (Research Genetics) with addition of internal amines, terminal biotin, or fluorophores. DNA hairpin-loop oligonucleotides of the type used to make M ('molecular beacons[20]') have a thymine in the loop region which was modified on the 5 position of the base with a C6 primary amine, to which a nanocrystal was covalently linked. 1.4-nm uncharged gold nanocrystals functionalized with a single sulpho *N*-hydroxy-succinimide (NHS) ester[29] (Nanoprobes) were incubated with the oligonucleotide in the manufacturer's buffer at room temperature for 1 h, resulting in a covalent bond between the nanocrystal and oligonucleotide[30]. Nanocrystals were in molar excess (>10 ×). Excess nanocrystals were removed by 70% ethanol precipitation on ice and repeated washes. The nanocrystals are soluble in ethanol, but the DNA or species attached to it precipitates. Gel electrophoresis is effective in separating nanocrystals from DNA-labelled gold nanocrystals, but for short DNA the mobility shift is expected to be too small to resolve the two species[24]. The concentration of M and N is 1×10^{-6} M in 1X PBS (1X PBS = 1 mM KH_2PO_4, 10 mM Na_2HPO_4, 137 mM NaCl, 2.7 mM KCl).

RFMF

Alternating magnetic fields were generated by applying an alternating current to a coil with 35 turns and a cross section of ~1 cm^2. Coils were wrapped around a plastic cuvette/tube holder with open structures to maximize light passage. Currents with $f = 1$ GHz were obtained using an RF signal generator (Hewlett Packard 8648C) with an output of 1 mW in conjunction with a linear amplifier. The ultimate output power range used was 0.4–4 W, though these are upper limits to the exact power inside the coil due to losses from set-up architecture (10% input power estimated to be transferred to coil). DNA hairpin samples (volume 200 μl) were in a 3 mm × 3 mm quartz cuvette inside the coil. The two-phase samples were in 250-μl plastic tubes (supernatant volume 165 μl, solid phase volume 60 μl) put into the coil in a water bath. The power used for the experiments shown in Figs 1 and 2 was 4 W, and 1 W for those in Fig. 3.

Spectroscopy

UV–visible spectra were taken on a DU530 Beckman spectrophotometer with time resolution limited to 5-s steps. Fluorescence spectra was taken on a Spex Fluoromax fluorometer with 1-nm steps, 0.1-s integration time, entrance/exit slits 1–5 nm, $\lambda_{excitation}$ = 450 nm. Signal was averaged multiple times (≤10). Fluorescence peak areas were quantified by Voigt lineshape deconvolution using a commercial program (Peakfit, SPSS). Figure 3b fits had the same parameters for peak positions and widths for both spectra.

Two-phase system

Molecule X is a 12-nucleotide DNA that has a 6-carboxyfluorescein (FAM, λ_{max} = 516 nm) on the 5′ end and a C6 primary amine on the 3′ end (T_m = 40 °C). It was labelled with the nanocrystal as described above. Molecule Y is a 68-nucleotide DNA complementary to X, and has a biotin on the 5′ end. X and Y were hybridized, and the X-Y hybrid was incubated with streptavidin agarose beads (Sigma-Aldrich) with $<d>$ = 100 μm to allow the biotin on Y to bind to streptavidin. Samples were washed several times with 1X PBS to remove free gold. This biotin–streptavidin reaction ($K_d = 10^{-15}$ M) is robust for the temperatures used here[30]. Tests in which bead-bound Y was heated to 85 °C showed no presence of oligonucleotide in the supernatant, confirming the biotin–streptavidin interaction was intact.

In the construction of the two-phase system (Fig. 2), X was purified from unlabelled oligonucleotides by exposing bead-immobilized X-Y to RFMF. Oligonucleotides not linked to a nanocrystal had no response to RFMF and thus remain hybridized to Y. This is another alternative to purification by gel electrophoresis[24]. Purified X was hybridized to Y, then exposed to streptavidin agarose beads to immobilize X-Y. After multiple washes with 1X PBS, buffer was added to the beads to serve as the liquid phase. Samples were exposed to RFMF or heated conventionally at a specific temperature for 5 min. Following heating or exposure to the RFMF, the supernatants were separated from the beads and then measured by fluorescence spectroscopy. All fluorescence spectra were taken under identical conditions (temperature, spectrometer parameters).

Mixed two-phase system

Oligonucleotide Z was identical in sequence to X but was labelled on the 3′ end with NHS-tetramethylrhodamine (TMR, Molecular Probes). Attachment of the TMR to the primary amine on Z was achieved by incubating the molecules together in sodium bicarbonate solutions (1 h, room temperature) in the dark to prevent photobleaching (manufacturer directions). Oligonucleotide Z was hybridized to Y, mixed in solution with X-Y, then incubated with tetrameric avidin acrylic beads (Sigma-Aldrich) as described above. Free molecules were removed with multiple washes of 1X PBS. The sample is equimolar in X to Z on the beads. The surface density of the monomeric avidin on the beads is ~1 molecule per nm^2.

Received 12 July; accepted 16 November 2001.

1. Ban, N., Nissen, P., Hansen, J., Moore, P. B. & Steitz, T. A. The complete atomic structure of the large ribosomal subunit at 2.4 Å resolution. *Science* **289,** 905–920 (2000).
2. Deniz, A. A. *et al.* Single-molecule protein folding: Diffusion fluorescence resonance energy transfer studies of the denaturation of chymotrypsin inhibitor 2. *Proc. Natl Acad. Sci. USA* **97,** 5179–5184 (2000).
3. Davenport, R., Wuite, G., Landick, R. & Bustamante, C. Single-molecule study of transcriptional pausing and arrest by *E. coli* RNA polymerase. *Science* **287,** 2497–2500 (2000).
4. Winfree, E., Liu, F., Wenzler, L. & Seeman, N. Design and self-assembly of two-dimensional DNA crystals. *Nature* **394,** 539–44 (1998).
5. Yurke, B. *et al.* A DNA-fuelled molecular machine made of DNA. *Nature* **406,** 605–608 (2000).
6. McAdams, H. H. & Arkin, A. Gene regulation: towards a circuit engineering discipline. *Curr. Biol.* **10,** R318–R320 (2000).
7. Elowitz, M. B. & Leibler, S. A synthetic oscillatory network of transcriptional regulators. *Nature* **403,** 335–338 (2000).
8. Whaley, S. R., English, D. S., Hu, E. L., Barbara, P. F. & Belcher, A. M. Selection of peptides with semiconductor binding specificity for directed nanocrystal assembly. *Nature* **405,** 665–668 (2000).
9. Telford, J. R., Wittung-Stafshede, P., Gray, H. B. & Winkler, J. R. Protein folding triggered by electron transfer. *Acc. Chem. Res.* **31,** 755–763 (1998).
10. Monroe, W. T., McQuain, M. M., Chang, M. S., Alexander, J. S. & Haselton, F. R. Targeting expression with light using caged DNA. *J. Biol. Chem.* **274,** 20895–20900 (1999).
11. Asanuma, H., Yoshida, T., Ito, T. & Komiyama, M. Photo-responsive oligonucleotides carrying azobenzene at the 2'-position of uridine. *Tetrahedr. Lett.* **40,** 7995–7998 (1999).
12. Liu, D., Karanicolas, J., Yu, C., Zhang, Z. & Woolley, G. A. Site-specific incorporation of photo-isomerizable azobenzene groups into Ribonuclease S. *Bioorg. Med. Chem. Lett.* **7,** 2677–2680 (1997).
13. Haupts, U., Tittor, J. & Oesterhelt, D. Closing in on bacteriorhodopsin: progress in understanding the molecule. *Annu. Rev. Biophys. Biomol. Struct.* **28,** 367–99 (1999).
14. Ashkenazi, G., Ripoll, D. R., Lotan, N. & Scheraga, H. A. A molecular switch for biochemical logic gates: Conformational studies. *Biosens. Bioelectron.* **12,** 85–95 (1997).
15. Hamad-Schifferli, K., Schwartz, J. J., Santos, A. T., Zhang, S. & Jacobson, J. M. in *Mater. Res. Soc. Proc.* (eds Hahn, H. W., Feldheim, D. L., Kubiak, C. P., Tannenbaum, R. & Siegel, R. W.) Y8.43 (MRS, San Francisco, 2001).
16. Lian, T., Locke, B., Kholodenko, Y. & Hochstrasser, R. M. Energy flow solute to solvent probed by femtosecond IR spectroscopy: malachite green and heme protein solutions. *J. Phys. Chem.* **98,** 11648–11656 (1994).
17. Orfeuil, M. *Electric Process Heating: Technologies/ Equipment/ Applications* (Battelle Press, Columbus, Ohio, 1987).
18. Zinn, S. & Semiatin, S. L. *Elements of Induction Heating, Design Control, and Applications* (ASM International, Materials Park, Ohio, 1988).
19. Hergt, R. *et al.* Physical limits of hyperthermia using magnetite fine particles. *IEEE Trans. Magn.* **34,** 3745–3754 (1998).
20. Bonnet, G., Tyagi, S., Libchaber, A. & Kramer, F. R. Thermodynamic basis of the enhanced specificity of structured DNA probes. *Proc. Natl Acad. Sci. USA* **96,** 6171–6176 (1999).
21. Taton, A. T., Mirkin, C. A. & Letsinger, R. L. Scanometric DNA array detection with nanoparticle probes. *Science* **289,** 1757–1760 (2000).
22. Loweth, C. J., Caldwell, W. B., Peng, X., Alivisatos, A. P. & Schultz, P. G. DNA-based assembly of gold nanocrystals. *Angew. Chem. Int. Edn Engl.* **38,** 1808–1812 (1999).
23. Mattoussi, H. *et al.* Self-assembly of CdSe-ZnS quantum dot bioconjugates using an engineered recombinant protein. *J. Am. Chem. Soc.* **122,** 12142–12150 (2000).
24. Zanchet, D., Micheel, C. M., Parak, W. J., Gerion, D. & Alivisatos, A. P. Electrophoretic isolation of discrete Au nanocrystal/DNA conjugates. *Nanoletters* **1,** 32–35 (2001).
25. Bonnet, G., Krichevsky, O. & Libchaber, A. Kinetics of conformational fluctuations in DNA hairpin-loops. *Proc. Natl Acad. Sci. USA* **95,** 8602–8606 (1998).
26. Cantor, C. R. & Schimmel, P. *Biophysical Chemistry* (Freeman, San Francisco, 1980).
27. Mao, C., LaBean, T. H., Reif, J. H. & Seeman, N. C. Logical computation using algorithmic self-assembly of DNA triple-crossover molecules. *Nature* **407,** 493–496 (2000).
28. Probst, J. C. Antisense oligodeoxynucleotide and ribozyme design. *Methods* **22,** 271–281 (2000).
29. Reardon, J. E. & Frey, P. A. Synthesis of undecagold cluster molecules as biochemical labeling reagents. 1. Monoacyl and mono[N-succinimidooxy)succinyl] undecagold clusters. *Biochemistry* **23,** 3849–3856 (1984).
30. Hermanson, G. T. *Bioconjugate Techniques* (Academic, San Diego, 1996).

Supplementary Information accompanies the paper on *Nature*'s website (http://www.nature.com).

Acknowledgements

We thank N. Afeyan, E. Lander and P. Matsudaira for discussions in the early stages of this work, and J.P. Shi for comments on the experimental work. This work was supported by DARPA and the MIT Media Lab TTT consortium.

Correspondence and requests for materials should be addressed to J.M.J. (e-mail: jacobson@media.mit.edu) or S.Z. (e-mail: shuguang@mit.edu).